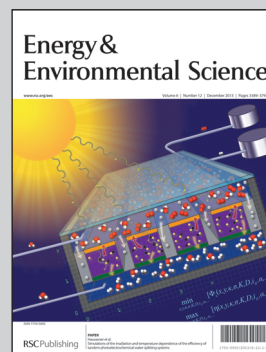


Showcasing the research of quantum dot sensitized solar cells from Prof. J. J. Tian's and Prof. G. Z. Cao's lab, University of Science and Technology, Beijing, China, and University of Washington, the United States.

**Title:** Architected ZnO photoelectrode for high efficiency quantum dot sensitized solar cells

We proposed a facile chemical passivation strategy for ZnO mesoporous photoelectrodes to improve the performance of a CdS/CdSe quantum dot co-sensitized solar cell (QDSC), which exhibited a high power conversion efficiency of 4.68%.

#### As featured in:



See Cao *et al.*,  
*Energy Environ. Sci.*, 2013, **6**, 3542.

## COMMUNICATION

## Architected ZnO photoelectrode for high efficiency quantum dot sensitized solar cells†

Cite this: *Energy Environ. Sci.*, 2013, **6**, 3542

Jianjun Tian,<sup>\*ac</sup> Qifeng Zhang,<sup>b</sup> Evan Uchaker,<sup>b</sup> Rui Gao,<sup>b</sup> Xuanhui Qu,<sup>a</sup> Shengen Zhang<sup>a</sup> and Guozhong Cao<sup>\*bc</sup>

Received 28th March 2013

Accepted 11th June 2013

DOI: 10.1039/c3ee41056k

[www.rsc.org/ees](http://www.rsc.org/ees)

In this work, we reported a facile chemical passivation strategy for a ZnO mesoporous photoelectrode to improve the performance of a CdS/CdSe quantum dot co-sensitized solar cell (QDSC). The QDSC exhibited a record power conversion efficiency of 4.68%.

Developing low-cost and high-performance solar devices for clean energy sources to replace fossil fuels is an urgent issue imposed on scientists around the world.<sup>1,2</sup> As a cost-effective alternative to silicon-based photovoltaics, quantum dot-sensitized solar cells (QDSCs) have attracted considerable attention recently and showed a promising development for next generation solar cells.<sup>2–6</sup> QDSCs can be regarded as a derivative of dye-sensitized solar cells (DSCs), however they use semiconductor quantum dots (QDs) as the photo-sensitizer instead of organic dyes.<sup>7–9</sup> Compared to organic dyes, QDs exhibit versatile optical and electrical properties, such as: (1) tunable band gap depending on the QD size, (2) larger extinction coefficient, (3) high stability toward water and oxygen, and (4) generation of multiple excitons with single-photon absorption.<sup>10–12</sup> The theoretical photovoltaic conversion efficiency of QDSCs can reach up to 44% in view of the multiple excitons generation (MEG) of QDs.<sup>12,13</sup>

Porous nanocrystalline TiO<sub>2</sub> is commonly used as the photoelectrode of QDSCs and its power conversion efficiency (PCE) has exceeded 4% according to several reports.<sup>12–15</sup> ZnO is known to have a similar energy-band structure and physical properties

**Broader context**

ZnO is considered one of the optimal candidate photoelectrodes for quantum dot sensitized solar cells (QDSCs) for its high electron mobility, suitable energy-band structure and excellent physical properties. However, the efficiency of ZnO based QDSCs is low, due to the diminished loading of QDs and high surface charge recombination. We developed a facile passivation strategy for a ZnO mesoporous photoelectrode. This method not only opened the apertures to improve the distribution of QDs in the photoelectrode, increased the specific surface area and reduced the surface defects of ZnO photoelectrodes to accommodate more QDs, but also suppressed the charge recombination and prolonged electron lifetime by introducing a barrier layer. As a result, a record power conversion efficiency of 4.68% was obtained. In addition, this passivation strategy can also be applied to dye sensitized solar cells and other photovoltaic devices to enhance their performances.

to TiO<sub>2</sub>. But it has a higher electron mobility.<sup>16–18</sup> Moreover, ZnO can easily form anisotropic structures, such as nanorods, nanowires and nanoflowers, which enables it to exhibit unique electronic and optical properties.<sup>19,20</sup> ZnO nanostructured photoelectrodes for QDSCs have been investigated over the last several years;<sup>21–25</sup> however, the efficiency of ZnO based QDSCs is lower than that of TiO<sub>2</sub> based devices, and is likely due to high surface charge recombination in ZnO.<sup>26</sup> The high surface charge recombination can be attributed to the many defects present on the ZnO surface, which ultimately boost the surface charge recombination. In addition, the chemical stability of ZnO is less than that of TiO<sub>2</sub>, which makes it easy for ZnO to react with the electrolyte. The instability also decreases the performance of the QDSC.<sup>27</sup> It has been demonstrated that the degree of charge recombination of DSCs can be effectively reduced by introducing a thin shell on the ZnO surface.<sup>28–32</sup> The shell usually has a more negative conduction band edge than that of ZnO or creates a dipole at the interface to shift the band edge so as to suppress surface charge recombination.<sup>30</sup> Although the charge recombination process in QDSCs is thought to be somewhat different from that in DSCs,<sup>33</sup> the method of introducing a thin shell as well as an energy barrier to prevent the electrons from

<sup>a</sup>Advanced Material and Technology Institute, University of Science and Technology Beijing, 100083, P.R. China. E-mail: [tianjianjun@mater.ustb.edu.cn](mailto:tianjianjun@mater.ustb.edu.cn); Fax: +86-10-62333375; Tel: +86-10-82376835

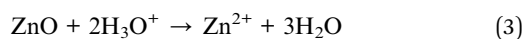
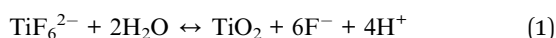
<sup>b</sup>Department of Materials and Engineering, University of Washington, Seattle, WA 98195-2120, USA. E-mail: [gzaoc@u.washington.edu](mailto:gzaoc@u.washington.edu); Fax: +1 206-543-3100; Tel: +1 206-616-9084

<sup>c</sup>Beijing Institute of Nanoenergy and Nanosystems, Chinese Academy of Sciences, 100083, P.R. China

† Electronic supplementary information (ESI) available: Experimental method, BET results, SEM and EDS of the film, *J*-*V* curve of the QDSC under dark conditions, electrochemical impedance results, recent reports for ZnO based efficiency of QDSCs. See DOI: 10.1039/c3ee41056k

transferring from the oxide to the electrolyte is believed to improve the performance of QDSCs effectively. In addition to forming an energy barrier, the shell can also change the surface energy of ZnO to load more QDs.<sup>26</sup>

This paper reports a facile chemical passivation strategy for a ZnO mesoporous photoelectrode, which not only enlarges the apertures in the ZnO mesoporous photoelectrode to harvest more QDs, but also introduces a thin TiO<sub>2</sub> nanoparticle layer on the surface of ZnO to decrease the surface charge recombination. The ZnO nanoparticle mesoporous films were immersed in an aqueous solution containing 0.04 M H<sub>3</sub>BO<sub>3</sub> and 0.1 M (NH<sub>4</sub>)<sub>2</sub>TiF<sub>6</sub> at room temperature for 30 min. The films were then washed several times with deionized water and annealed at 400 °C (detailed information is provided in the ESI†). Such treatment leads to the formation of a thin passivation layer on the surface of the ZnO nanoparticles. The passivation process can be expressed *via* the following equations:<sup>34</sup>



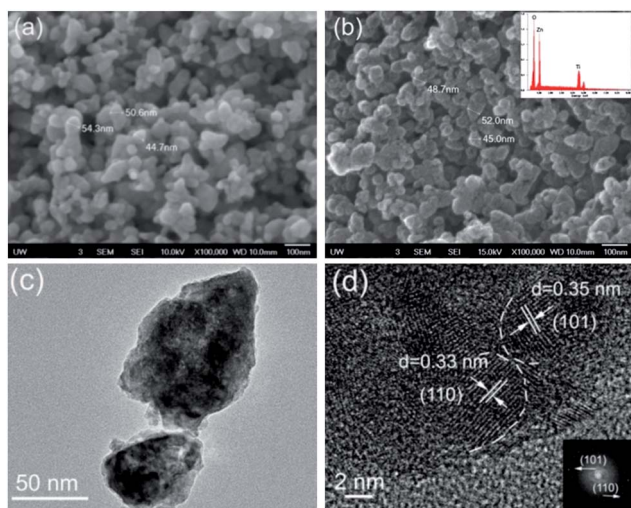
Reactions (1) and (2) can be shifted to the right by reaction (3), which indicates that dissolution of ZnO can boost the hydrolyzation of TiF<sub>6</sub><sup>2-</sup>. With the dissolution of ZnO, TiO<sub>2</sub> nanoparticles are gradually deposited on the fresh surface of ZnO.

Fig. 1a and b show scanning electron microscopy (SEM) images of the ZnO mesoporous films without and with the passivation layer, respectively. It can be seen that the surfaces of the passivated ZnO nanoparticles appear rough and tarnished, while the particle size remains nearly the same as the unpassivated ZnO nanoparticles. Energy-dispersive X-ray spectroscopy (EDS) (shown in Fig. 1b inset) shows the presence of O, Zn

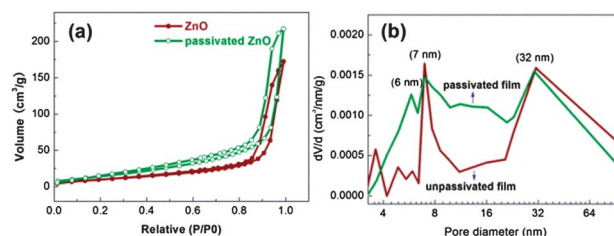
and Ti elements, indicating the formation of the TiO<sub>2</sub> layer on the surface of passivated ZnO nanoparticles. Fig. 1c and d show TEM and HRTEM images of the passivated ZnO mesoporous film, which demonstrate that the ZnO particles ranging from 40 to 60 nm are coated with the small particles. The diameter of the small particles is approximately 4 nm. The small particles are identified as TiO<sub>2</sub> by both lattice constant (shown in Fig. 1d) and FFT diffraction pattern (shown in Fig. 1d inset).

Fig. 2 shows nitrogen adsorption–desorption isotherms and the BJH (Barrett–Joyner–Halenda) pore size distribution of ZnO films after and before passivation. The multi-point Brunauer–Emmett–Teller (BET) method is used to determine the specific surface area. For QDSCs, the size and distribution of the mesopores affect the loading and distribution of QDs in the photoelectrode. The BJH method is used to measure the diameter and distribution of mesopores, the results of which are listed in Table S1 (shown in the ESI†). It can be seen that there is an increase in the specific surface area and the mesopore volume from 57.7 m<sup>2</sup> g<sup>-1</sup> and 0.342 cm<sup>3</sup> g<sup>-1</sup> for the unpassivated film to 68.6 m<sup>2</sup> g<sup>-1</sup> and 0.401 cm<sup>3</sup> g<sup>-1</sup> for the passivated one, respectively. However, the average mesopore diameter of the passivated film (29.7 nm) is slightly less than that of the unpassivated film (31.3 nm). It can be inferred that the quantity of the passivated mesopore film increases due to the increase of the total volume and decrease of the average pore diameter. Fig. 2b shows the distribution of the mesopores in the films. Compared to the distribution curve of the unpassivated film, the distribution peaks of the pores with size below 6 nm in the passivated film disappear. In addition, the surface state of ZnO nanoparticles has been changed by the passivation process. Erdem *et al.*<sup>35</sup> reported that the surface defects of ZnO could be reduced by forming a core/shell, which would be loading of QDs.

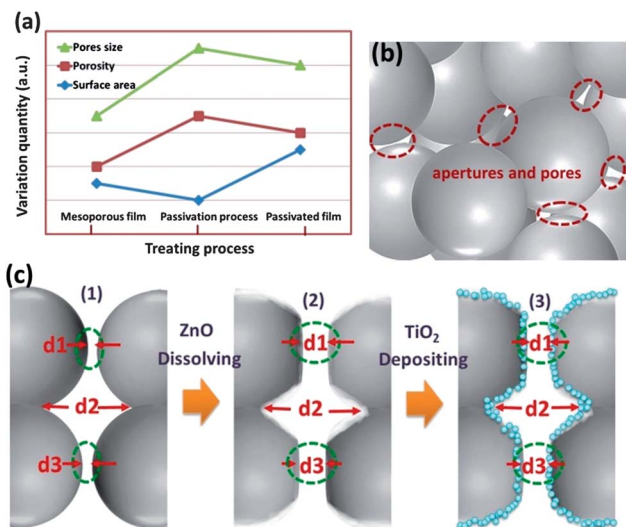
Scheme 1a illustrates the variation of the pore size, porosity and surface area of the film during the passivation process. At first, ZnO is dissolved by reacting with H<sub>3</sub>O<sup>+</sup> so as to open the apertures and pores (shown in Scheme 1b), leading to the increase in the porosity and pore size of the film; however, the specific surface area of the film slightly decreases. Upon depositing TiO<sub>2</sub> onto the surface of ZnO, the porosity and pore size experience little reduction while the specific surface area of the film increases. Finally, the porosity, size of dominant pores and specific surface area of the film are improved after the passivation process. These changes are consistent with the results from BET. Scheme 1c shows schematic diagrams of the ZnO mesoporous film passivation process. During the



**Fig. 1** SEM images of (a) ZnO and (b) passivated ZnO mesoporous films, the inset shows the EDS image; (c) TEM and (d) HRTEM images of the passivated ZnO mesoporous film, the inset shows the FFT diffraction pattern of small particles.



**Fig. 2** (a) Nitrogen adsorption–desorption isotherms and (b) BJH pore size distribution plots.



**Scheme 1** (a) Variation of the pore size, porosity and surface area of the film during the passivation process, (b) apertures and pores of the mesoporous film, (c) passivation process of the ZnO mesoporous film.

passivation process, all of the ZnO exposed facets can be etched in chemical solution, which increases  $d_1$ ,  $d_2$  and  $d_3$ . However, the reacting ions (e.g.  $H_3O^+$ ) tend to concentrate on the high-energy surface in an attempt to reduce the total surface energy.<sup>36</sup> Since a convex surface has higher surface energy ( $\gamma_v$ ) and higher solubility than a concave surface ( $\gamma_c$ ) for a given material,<sup>36</sup> the convex surface of ZnO is originally etched and dissolved. This dissolution process opens the apertures and enlarges the small pores ( $d_1$  and  $d_3$ ), thus allowing the QD precursor solution to enter the inner pores easily and distribute homogeneously within the photoelectrode film. Although  $\gamma_c$  is lower than  $\gamma_v$ ,  $d_2$  is still greater than  $d_1$  and  $d_3$ . While dissolving the ZnO, TiO<sub>2</sub> particles deposit on the fresh surface and combine with the newly broken chemical bonds. As a result, the ZnO particles are fully coated by the precipitation, as shown in the schematic drawing (3) of Scheme 1c. The simultaneous deposition of TiO<sub>2</sub> nanoparticles not only changes the surface chemistry of the photoelectrode to favour high loading of QDs, but also functions as an energy barrier layer to suppress surface charge recombination.

To examine the effect of the passivation process on the porosity and QD loading of the photoelectrodes, the QD distribution within the ZnO film has been studied. Fig. S1a (shown in the ESI†) shows a cross-sectional image of the ZnO film. The mapping images of Se and S along the cross-section are shown in Fig. 3a–d. The distribution curves and data of Se and S in the different depths are shown in Fig. S1b and c and listed in Table S2, respectively (shown in the ESI†). It can be seen that, for the unpassivated ZnO mesoporous film, Se and S are mainly concentrated on the upper section of the photoelectrode film and their profile decreases gradually towards the bottom of the film, indicating that it is difficult for the QD precursor to penetrate into the deep pores. In contrast, Se and S in the passivated photoelectrode present a much more uniform and homogeneous distribution, in view of the enlarged apertures

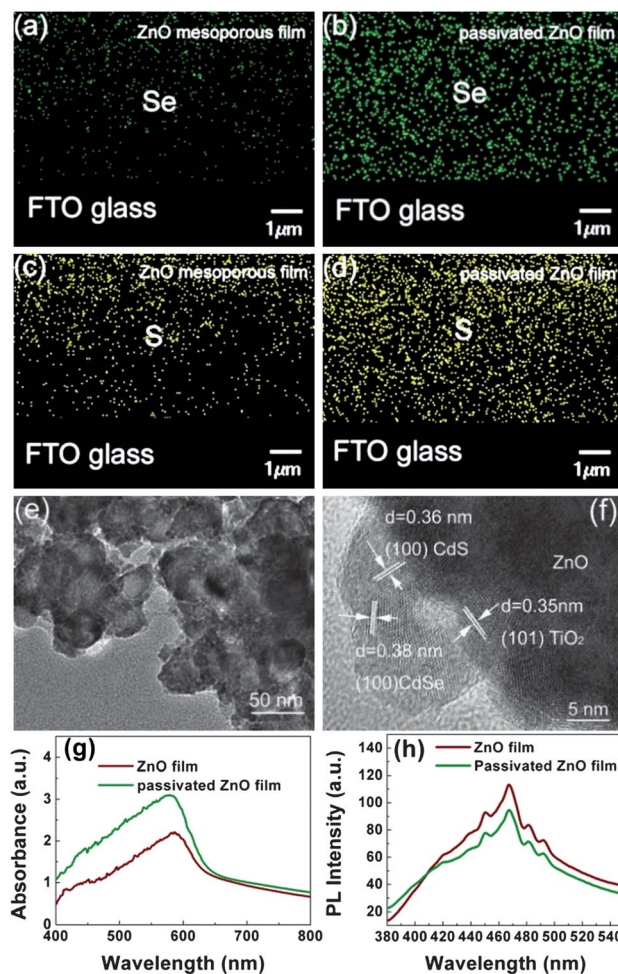


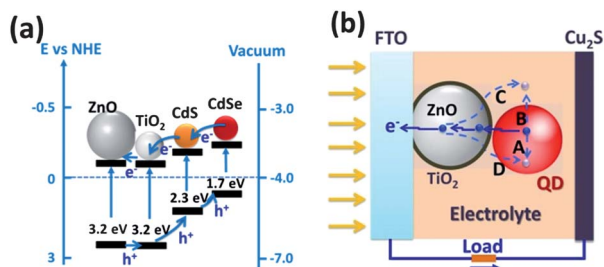
**Fig. 3** EDS mapping images of Se in (a) unpassivated and (b) passivated ZnO films, S in (c) unpassivated and (d) passivated ZnO films, (e) TEM and (f) HRTEM images of passivated ZnO films loaded with QDs, (g) UV-Vis spectra curves of the ZnO films loaded with QDs and (h) photoluminescence (PL) spectra curves of ZnO films.

and increased porosity of the passivated film. Fig. 3e and f display the TEM and HRTEM images of the passivated ZnO loaded with QDs, showing ZnO coated with TiO<sub>2</sub> nanoparticles surrounded by CdS/CdSe QDs that are 4–6 nm in size. These images indicate that the QDs (4–6 nm) can enter into the interior and bottom of the passivated film, and distribute homogeneously throughout the passivated film. Fig. 3g compares the absorbance of the passivated and unpassivated ZnO films loaded with QDs. The high absorbance of the passivated ZnO film indicates that more QDs were successfully loaded. Fig. 3h presents the typical PL spectra curves of ZnO films under an excitation wavelength of 320 nm, which exhibit a broad emission with peak intensity at 467 nm. The PL intensity of the passivated ZnO film is less than that of the unpassivated ZnO film. The emission intensity of ZnO depends on the surface defects<sup>37</sup> and the low emission intensity of the passivated ZnO film proves that the amount of surface defects is indeed reduced. In view of the above results, it is evident that the passivation process not only opens the apertures and pores for homogeneous QD distribution within the photoelectrode, but

also reduces the surface defects by depositing a TiO<sub>2</sub> nanoparticle layer to accommodate more QDs.

The effects of the passivation layer on the surface charge transport and recombination are illustrated in Scheme 2. Scheme 2a shows the values of the conduction bands (CB): CdSe > CdS > ZnO > TiO<sub>2</sub>.<sup>38,39</sup> The CdS/CdSe QD sensitizer has a type II band alignment. Under the operating conditions, photons are captured by the QDs, yielding electron-hole pairs that are rapidly separated. The electrons inject into the TiO<sub>2</sub> CB and then transfer into the ZnO CB. The holes remaining in the QDs are reduced by redox couples (S<sup>2-</sup>/S<sub>n</sub><sup>2-</sup>) in the electrolyte. As a barrier layer, the passivation layer suppresses recombination of electrons with holes in the electrolyte.<sup>30</sup> As for recombination in QDSCs, a schematic diagram for the recombination pathways on the basis of former reports<sup>31,34-36</sup> is shown in Scheme 2b: (A) recombination of electrons in the QD conduction band and holes in the QD valence band; (B) recombination of electrons with the electron acceptors in the electrolyte; (C) back electron injection from ZnO to the electrolyte; (D) back electron injection from ZnO to QDs. Among these pathways, processes (A) and (B) can be ignored due to the highly efficient charge separation.<sup>26</sup> Recombination pathways (C) and (D) can be considered as the main factors that affect the performance of a QDSC, and depend on the photoelectrode/QDs/electrolyte interfacial resistance. The TiO<sub>2</sub> passivation layer can increase the interfacial resistance and lead to recombination reduction through the mechanisms (C) and (D). Fig. S2 (shown in the ESI†) presents the photocurrent-voltage (*J*-*V*) curves of the QDSCs assembled with ZnO and passivated ZnO films under dark conditions. The dark current of the passivated ZnO photoelectrode device decreases compared to that of the unpassivated ZnO photoelectrode, which is indicative of a lower charge recombination from the ZnO CB back to the redox couple (S<sup>2-</sup>/S<sub>n</sub><sup>2-</sup>) in the electrolyte, and is ascribed to the increase of recombination resistance of pathways (C) and (D).<sup>26</sup>

To evaluate the resistance distribution and charge recombination processes, electrochemical impedance spectroscopy (EIS) measurements have been carried out. Fig. 4a and b show the impedance spectra of the QDSCs measured under dark conditions with a forward bias of -0.6 V. The fitting results of the impedance spectra are listed in Table S3 (shown in the ESI†). In Fig. 4a, the semicircle represents the electron transfer at the photoelectrode/QDs/electrolyte interface and transport in the photoelectrode (*R*<sub>ct</sub>).<sup>40</sup> The *R*<sub>ct</sub> of the passivated ZnO based



**Scheme 2** (a) Energy band structure of ZnO/TiO<sub>2</sub>/CdS/CdSe<sup>38,39</sup> and (b) surface charge recombination pathways of the QDSC.

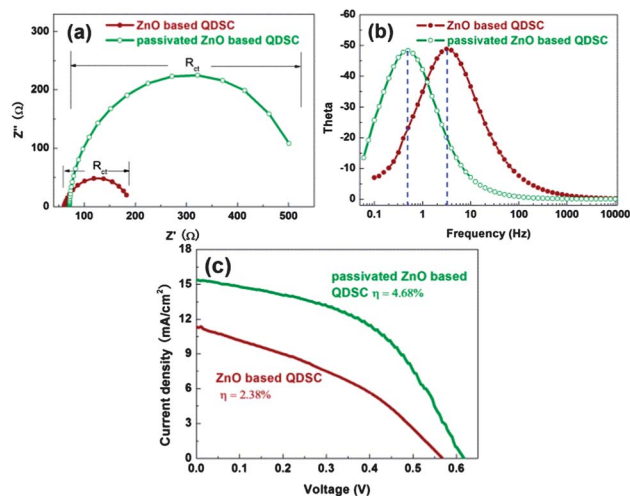


**Fig. 4** (a) Nyquist plot curves and (b) Bode plot curves of the QDSCs under forward bias (-0.6 V) and dark conditions, and (c) *J*-*V* curves of QDSCs under simulated AM 1.5, 100 mW cm<sup>-2</sup> sunlight.

QDSC is 470.3 Ω, which is more than twice that of the unpassivated ZnO device (131.6 Ω). The charge transfer resistance at the photoelectrode/electrolyte interface (*R*<sub>ct</sub>) is determined by both the ZnO and TiO<sub>2</sub> passivation layer, and the total charge transfer resistance can be written using eqn (4):<sup>28</sup>

$$R_{\text{total}} = R_{\text{ZnO}} + R_{\text{TiO}_2} \quad (4)$$

where *R*<sub>ZnO</sub> and *R*<sub>TiO<sub>2</sub></sub> are the electron transfer resistances induced by the ZnO and TiO<sub>2</sub> passivation layer, respectively. EIS results indicate that recombination of electrons in the ZnO photoelectrode, with the passivation layer, with holes in the electrolyte is a more difficult process in view of its high *R*<sub>ct</sub>. *R*<sub>ct</sub> can be considered as part of a shunt resistance (*R*<sub>sh</sub>) because it behaves like a diode with the applied bias voltage.<sup>28</sup> *R*<sub>sh</sub> relates to the FF according to the following eqn (5):<sup>28</sup>

$$\text{FF} = \text{FF}_0(1 - 1/R_{\text{sh}}) \quad (5)$$

where FF<sub>0</sub> is the theoretical maximum FF. It can be inferred that the increase in FF of the QDSC assembled with the passivated photoelectrode is a result of an increase in *R*<sub>sh</sub>. The increase of interfacial resistance also indicates that the surface defects of ZnO are reduced by the passivation process, which is in good agreement with the results presented in Fig. 3h. Fig. 4b shows the Bode plots of the QDSCs with the different photoelectrodes. The curve peak of the spectrum can be used to determine the electron lifetime in the ZnO (according to the equation  $\tau_n = 1/(2\pi f_{\text{min}})$ ).<sup>41</sup> It is clear that the electron lifetime for the device with the passivated ZnO photoelectrode, 317.9 ms, is much longer than the 50.4 ms electron lifetime for the unpassivated ZnO. The electron lifetime ( $\tau_n$ ) is directly proportional to *R*<sub>ct</sub> and is calculated using eqn (6):<sup>42</sup>

$$\tau_n = R_{\text{ct}} C_{\mu} \quad (6)$$

where *C*<sub>μ</sub> is the corresponding chemical capacitance. Consequently, employment of the passivating layer can enhance the

**Table 1** Properties of ZnO and passivated ZnO based QDSCs<sup>a</sup>

Samples	$V_{oc}$ (V)	$J_{sc}$ (mA cm <sup>-2</sup> )	FF	$\eta$ (%)
ZnO	0.57 ± 0.03	11.61 ± 0.25	0.36 ± 0.02	2.38 ± 0.11
Passivated ZnO	0.62 ± 0.02	15.42 ± 0.23	0.49 ± 0.02	4.68 ± 0.08

<sup>a</sup> The standard deviation of the properties is based on the data of 3 cells.

charge recombination resistance and thus prolong the electron lifetime.<sup>28,29</sup> Thus, employment of the passivation layer not only increases the amount of harvesting QDs and improves their distribution, but may also enhance the charge recombination resistance and prolong the electron lifetime, which both contribute to improving the  $J_{sc}$ , FF and  $V_{oc}$  of QDSCs. Fig. 4c shows the  $J$ - $V$  curves for the solar cells measured under the illumination of one sun (AM 1.5, 100 mW cm<sup>-2</sup>). The performance parameters of the solar cells are listed in Table 1, where it is apparent that the passivated ZnO based QDSC exhibits high performance:  $J_{sc} = 15.4$  mA cm<sup>-2</sup>,  $V_{oc} = 0.62$  V, FF = 0.49 and  $\eta = 4.68\%$ . Compared with the unpassivated photoelectrode, the passivated ZnO photoelectrode presents increases in  $V_{oc}$ ,  $J_{sc}$ , FF and  $\eta$  of 33%, 9%, 36% and 97%, respectively. To our knowledge, the  $\eta$  of 4.68% and FF of 0.49 are some of the highest respective values for ZnO based QDSCs at this time (Table S4, ESI†). In addition, the QDSCs have good stability in ambient conditions (shown in Fig. S3†).

## Conclusions

A passivation strategy for a ZnO mesoporous photoelectrode for a CdS/CdSe quantum dot co-sensitized solar cell (QDSC) was developed and the resulting QDSC exhibited a record power conversion efficiency of 4.68%. The passivation process offered several advantages to QDSCs as follows: (1) opens the apertures by dissolving the ZnO surface to improve QD distribution within the photoelectrode, (2) increases the specific surface area and reduces the surface defects by depositing a TiO<sub>2</sub> nanoparticle layer to accommodate more QDs, and (3) suppresses the charge recombination by preventing electrons in the ZnO conduction band from transferring to the oxidized ions in the electrolyte, which leads to prolonged electron lifetime. As a result, the ZnO based QDSC exhibited a high  $J_{sc}$  of 15.4 mA cm<sup>-2</sup>,  $V_{oc}$  of 0.62 V and efficiency ( $\eta$ ) of 4.68% under simulated AM 1.5, 100 mW cm<sup>-2</sup>.

## Acknowledgements

This work was supported by the National Science Foundation of China (51004011 and 51174247), and the Fundamental Research Funds for the Central Universities (FRF-TP-12-153A), and the U.S. Department of Energy, Office of Basic Energy Sciences, Division of Materials Sciences, under Award no. DE-FG02-07ER46467 (Q.F.Z.). This work is also supported in part by the National Science Foundation (DMR 1035196), the University of Washington TGIF grant, and the Royalty Research Fund (RRF) from the Office of Research at the University of Washington.

## Notes and references

- 1 M. Graetzel, R. A. J. Janssen, D. B. Mitzi and E. H. Sargent, *Nature*, 2012, **488**, 304–312.
- 2 H. Tada, M. Fujishima and H. Kobayashi, *Chem. Soc. Rev.*, 2011, **40**, 4232–4243.
- 3 P. K. Santra and P. V. Kamat, *J. Am. Chem. Soc.*, 2012, **134**, 2508–2511.
- 4 M. A. Hossain, J. R. Jennings, Z. Y. Koh and Q. Wang, *ACS Nano*, 2011, **5**, 3172–3181.
- 5 J. Ryu, S. H. Lee, D. H. Nam and C. B. Park, *Adv. Mater.*, 2011, **23**, 1883–1888.
- 6 T. Sugaya, O. Numakami, R. Oshima, S. Furue, H. Komaki, T. Amano, K. Matsubara, Y. Okano and S. Niki, *Energy Environ. Sci.*, 2012, **5**, 6233–6237.
- 7 J. H. Bang and P. V. Kamat, *Adv. Funct. Mater.*, 2010, **20**, 1970–1976.
- 8 V. Gonzalez-Pedro, X. Xu, I. Mora-Sero and J. Bisquert, *ACS Nano*, 2010, **4**, 5783–5790.
- 9 X.-Y. Yu, J.-Y. Liao, K.-Q. Qiu, D.-B. Kuang and C.-Y. Su, *ACS Nano*, 2011, **5**, 9494–9500.
- 10 G. Zhu, L. Pan, T. Xu and Z. Sun, *ACS Appl. Mater. Interfaces*, 2011, **3**, 3146–3151.
- 11 Y. L. Lee and Y. S. Lo, *Adv. Funct. Mater.*, 2009, **19**, 604–609.
- 12 J. J. Tian, R. Gao, Q. F. Zhang, S. G. Zhang, Y. W. Li, J. L. Lan, X. H. Qu and G. Z. Cao, *J. Phys. Chem. C*, 2012, **116**, 18655–18662.
- 13 T. L. Li, Y. L. Lee and H. Teng, *Energy Environ. Sci.*, 2012, **5**, 5315–5324.
- 14 M. A. Hossain, J. R. Jennings, C. Shen, J. H. Pan, Z. Y. Koh, N. Mathews and Q. Wang, *J. Mater. Chem.*, 2012, **22**, 16235–16242.
- 15 Z. X. Pan, H. Zhang, K. Cheng, Y. M. Hou, J. L. Hua and X. H. Zhong, *ACS Nano*, 2012, **6**, 3982–3991.
- 16 T. P. Chou, Q. F. Zhang, G. E. Fryxell and G. Z. Cao, *Adv. Mater.*, 2007, **19**, 2588–2592.
- 17 Q. F. Zhang and G. Z. Cao, *J. Mater. Chem.*, 2011, **21**, 6769–6774.
- 18 Q. F. Zhang, T. R. Chou, B. Russo, S. A. Jenekhe and G. Z. Cao, *Angew. Chem., Int. Ed.*, 2008, **47**, 2402–2406.
- 19 Q. F. Zhang, C. S. Dandeneau, X. Y. Zhou and G. Z. Cao, *Adv. Mater.*, 2009, **21**, 4087–4108.
- 20 Q. F. Zhang, S. Yodyingyong, J. T. Xi, D. Myers and G. Z. Cao, *Nanoscale*, 2012, **4**, 1436–1445.
- 21 M. Seol, H. Kim, Y. Tak and K. Yong, *Chem. Commun.*, 2010, **46**, 5521–5523.
- 22 M. Seol, E. Ramasamy, J. Lee and K. Yong, *J. Phys. Chem. C*, 2011, **115**, 22018–22024.
- 23 C.-Z. Yao, B.-H. Wei, L.-X. Meng, H. Li, Q.-J. Gong, H. Sun, H.-X. Ma and X.-H. Hu, *J. Power Sources*, 2012, **207**, 222–228.
- 24 T. Bora, H. H. Kyaw and J. Dutta, *Electrochim. Acta*, 2012, **68**, 141–145.
- 25 H. M. Cheng, K. Y. Huang, K. M. Lee, P. Yu, S. C. Lin, J. H. Huang, C. G. Wu and J. Tang, *Phys. Chem. Chem. Phys.*, 2012, **14**, 13539–13548.
- 26 J. J. Tian, Q. F. Zhang, L. L. Zhang, R. Gao, L. F. Shen, S. G. Zhang, X. H. Qu and G. Z. Cao, *Nanoscale*, 2013, **5**, 936–943.

- 27 A. Irannejad, K. Janghorban, O. K. Tan, H. Huang, C. K. Lim, P. Y. Tan, X. Fang, C. S. Chua, S. Maleksaeedi, S. M. H. Hejazi, M. M. Shahjamali and M. Ghaffari, *Electrochim. Acta*, 2011, **58**, 19–24.
- 28 K. Park, Q. F. Zhang, B. B. Garcia and G. Z. Cao, *J. Phys. Chem. C*, 2011, **115**, 4927–4934.
- 29 K. Park, Q. F. Zhang, B. B. Garcia, X. Y. Zhou, Y. H. Jeong and G. Z. Cao, *Adv. Mater.*, 2010, **22**, 2329–2332.
- 30 M. Law, L. E. Greene, A. Radenovic, T. Kuykendall, J. Liphardt and P. D. Yang, *J. Phys. Chem. B*, 2006, **110**, 22652–22663.
- 31 M. L. Wang, C. G. Huang, Y. G. Cao, Q. J. Yu, Z. H. Deng, Y. Liu, Z. Huang, J. Q. Huang, Q. F. Huang, W. Guo and J. K. Liang, *J. Phys. D: Appl. Phys.*, 2009, **42**, 155104.
- 32 N. O. V. Plank, I. Howard, A. Rao, M. W. B. Wilson, C. Ducati, R. S. Mane, J. S. Bendall, R. R. M. Louca, N. C. Greenham, H. Miura, R. H. Friend, H. J. Snaith and M. E. Welland, *J. Phys. Chem. C*, 2009, **113**, 18515–18522.
- 33 I. Mora-Sero, S. Gimenez, F. Fabregat-Santiago, R. Gomez, Q. Shen, T. Toyoda and J. Bisquert, *Acc. Chem. Res.*, 2009, **42**, 1848–1857.
- 34 S. Yodyingyong, X. Y. Zhou, Q. F. Zhang, D. Triampo, J. T. Xi, K. Park, B. Limketkai and G. Z. Cao, *J. Phys. Chem. C*, 2010, **114**, 21851–21855.
- 35 S. K. S. Parashar, B. S. Murty, S. Repp, S. Weber and E. Erdem, *J. Appl. Phys.*, 2012, **111**, 113712.
- 36 G. Cao and Y. Wang, *Nanostructures and Nanomaterials*, World Scientific Publishing Co. Pte. Ltd., Singapore, 2011.
- 37 H. Zeng, G. Duan, Y. Li, S. Yang, X. Xu and W. Cai, *Adv. Funct. Mater.*, 2010, **20**, 561–572.
- 38 Y. Xu and M. A. A. Schoonen, *Am. Mineral.*, 2000, **85**, 543–556.
- 39 L.-W. Chong, H.-T. Chien and Y.-L. Lee, *J. Power Sources*, 2010, **195**, 5109–5113.
- 40 N. Koide, A. Islam, Y. Chiba and L. Y. Han, *J. Photochem. Photobiol., A*, 2006, **182**, 296–305.
- 41 R. Kern, R. Sastrawan, J. Ferber, R. Stangl and J. Luther, *Electrochim. Acta*, 2002, **47**, 4213–4225.
- 42 Q. Wang, S. Ito, M. Gratzel, F. Fabregat-Santiago, I. Mora-Sero, J. Bisquert, T. Bessho and H. Imai, *J. Phys. Chem. B*, 2006, **110**, 25210–25221.